A potential-of-mean-force approach for fracture mechanics of heterogeneous materials using the lattice element method

Hadrien Laubie, Farhang Radjai, Roland Pellenq, Franz-Josef Ulm

A potential-of-mean-force approach for fracture mechanics of heterogeneous materials using the lattice element method

Hadrien Laubie [a], Farhang Radjaï [b, c], Roland Pellenq [a, b, d], Franz-Josef Ulm [a, b, *]

[a] Department of Civil and Environmental Engineering, Massachusetts Institute of Technology, Cambridge, MA 02139, USA
[b] ⟨ MSE⟩ [2], UMI 3466 CNRS - MIT Energy Initiative, Massachusetts Institute of Technology, 77 Massachusetts Avenue, Cambridge 02139, USA
[c] LMGC, UMR 5508 CNRS - Université de Montpellier, 163 rue Auguste Broussonnet, 34090 Montpellier, France
[d] CINaM, CNRS - Aix Marseille Université, Campus de Luminy, 13288 Marseille Cedex 09, France

A B S T R A C T

Fracture of heterogeneous materials has emerged as a critical issue in many engineering applications, ranging from subsurface energy to biomedical applications, and requires a rational framework that allows linking local fracture processes with global fracture descriptors such as the energy release rate, fracture energy and fracture toughness. This is achieved here by means of a local and a global potential-of-mean-force (PMF) inspired Lattice Element Method (LEM) approach. In the local approach, fracture-strength criteria derived from the effective interaction potentials between mass points are shown to ex- hibit a scaling commensurable with the energy dissipation of fracture processes. In the global PMF-approach, fracture is considered as a sequence of equilibrium states associated with minimum potential energy states analogous to Griffith's approach. It is found that this global approach has much in common with a Grand Canonical Monte Carlo (GCMC) approach, in which mass points are randomly removed following a maximum dissipa- tion criterion until the energy release rate reaches the fracture energy. The duality of the two approaches is illustrated through the application of the PMF-inspired LEM for fracture propagation in a homogeneous linear elastic solid using different means of evaluating the energy release rate. Finally, by application of the method to a textbook example of frac- ture propagation in a heterogeneous material, it is shown that the proposed PMF-inspired LEM approach captures some well-known toughening mechanisms related to fracture en- ergy contrast, elasticity contrast and crack deflection in the considered two-phase layered composite material.

Keywords:
Inhomogeneous material
Elastic material
Crack branching and bifurcation
Crack propagation and arrest
Fracture mechanisms
Fracture toughness

1. Introduction

Fracture Mechanics deals with the fracture resistance of solids subject to load. In its continuum version, it either follows a global or a local approach using concepts of linear or non-linear elastic fracture mechanics. The global approach was set in stone by Griffith (1921) as the irreversible dissipation of potential energy by means of fracture surface creation; the second by Irwin's stress concentration approach (Irwin, 1958) that recognizes that stress singularities at the crack tip

* Corresponding author at: ⟨*MSE*⟩[2], UMI 3466 CNRS - MIT Energy Initiative, Massachusetts Institute of Technology, 77 Massachusetts Avenue, Cambridge 02139, USA.
E-mail addresses: hlaubie@mit.edu (H. Laubie), fradjai@mit.edu (F. Radjaï), pellenq@mit.edu (R. Pellenq), ulm@mit.edu (F.-J. Ulm).

have some characteristic asymptotic patterns which permit prediction of fracture propagation. Both approaches have been extended since the 1960s far into the regime of non-linear behavior of solids (starting with the works of Barenblatt, 1962; Bažant, 1984; Dugdale, 1960; Hutchinson, 1968; Rice and Thomson, 1974 and many more). These methods, however, developed for homogeneous materials. It is well known that the microstructure of heterogeneous solids can contribute to their toughness, that is the increase of their fracture resistance induced by their local micro-texture. These mechanisms were notably observed in natural hierarchical composite materials such as nacre (see e.g. Kamat et al., 2000) or bones (see e.g. Launey et al., 2010) and several microstructure-based fracture mechanics models were derived. They include toughening due to microcracks (Shum and Hutchinson, 1990), crack bridging by uncracked stiff or tough inclusion (Bower and Ortiz, 1991) or layers (Shao et al., 2012), crack front roughening (Gao and Rice, 1989) or crack deflection (Faber and Evans, 1983; He and Hutchinson, 1989). All these theoretical works were, however, applied to specific inhomogeneous morphologies and spatial configurations. Recent developments in imaging techniques such as micro-computed tomography now give access to the full microstucture of real materials but in order to assess their failure behavior, new numerical tools must be introduced. Different methods have been used for the numerical study of heterogeneous solids. The weight-function theory of Rice (1985) and Bueckner (1987) was used by e.g. Démery et al. (2014). However, this approach is more suited to the study of planar crack propagation. Direct application of the finite element method (FEM) to complex microtextures is possible in theory but requires cumbersome remeshing techniques and may become too computationally demanding. More recent extended formulations of the FEM technique such as the XFEM are yet not well adapted to complex problems involving crack nucleation or crack branching phenomena (Sukumar et al., 2015). Such restrictions are absent from recent variational-based approaches (Bourdin et al., 2010). Phase-field models for fracture of brittle solids that emerged from this pioneering work were promisingly applied to heterogeneous solids (see e.g. Hossain et al., 2014; Nguyen et al., 2015). A persistent question yet remains as to the application of fracture mechanics methods to discrete material systems, despite the growing number of applications ranging from molecular scale (for an overview on the topic see Brochard et al., 2015 and references cited herein) to meso-scale of heterogeneous materials (for a recent review, see Bonamy and Bouchaud, 2011).

The simplest discrete system in solid mechanics is a lattice-type discretization (Hrennikoff, 1941), whose algorithmic implementation was first coined by Topin et al. (2007) as the Lattice Element Method (LEM); which is why this paper will focus on this method. The method emerged congruently in computational solid mechanics and statistical mechanics as a truss-beam-type discretization of a solid for both 2-D and 3-D problems, including strength and fracture investigations of random media using regular or irregular networks (Herrmann and Roux, 1990), which were applied to a large range of heterogeneous materials ranging from particle composites and cemented aggregates to concrete, ceramics and interface cracks in masonry composites (Nayfeh and Hefzy, 1978; Hansen et al., 1989; van Mier, 1996; Schlangen and Garboczi, 1996; Chiaia et al., 1997; Schlangen and Garboczi, 1997; Bolander Jr and Saito, 1998; van Mier et al., 2002; Lilliu and van Mier, 2003; Topin et al., 2007; Affes et al., 2012; Mohammadipour and Willam, 2015; 2016). While these applications to a large range of heterogeneous material systems evidence the suitability of LEM to investigate local rupture, fracture surface generation, fracture coalescence, percolation, and crack deflection, most investigations employ local link-failure criteria based on strength criteria that rest upon the assumption that link elements break at a given stress or force-moment strength criteria, independent of the discretization. Such local strength-based approaches are expected to fail to capture size effects associated with fracture that result from the intrinsic competition between bulk dissipation (related to strength) and surface dissipation that defines fracture.

With these limitations in mind, this paper proposes a framework that can tackle the duality of the global and the local fracture mechanics approach in the context of discrete simulations of solids using LEM. The starting point of this approach is the realization that LEM can be viewed as a potential-of-mean-force approach (PMF) akin to the one employed by the soft-matter physics community: a number of mass points defined on a regular or irregular lattice interact via effective potentials from which forces and moments derive. This PMF approach to LEM was recently proposed for elastic systems (Laubie et al., 2017a; 2017b), showing that the elasticity in the PMF context is but an evaluation of the energy content of the system around the equilibrium state defined by the lattice structure, for which most non-harmonic potentials degenerate to harmonic potentials commensurable to the original truss-beam type formulation used in classical LEM approaches. On the other hand, the PMF approach puts the LEM on the same footing as molecular approaches thus permitting to employ the canon of statistical physics, such as thermodynamic ensemble definitions, to extend the LEM approach as a tool of solid mechanics to poromechanics (Monfared et al., 2017). By considering the PMF-approach for fracture modeling of homogeneous and heterogeneous systems, the purpose of this paper is to extend our earlier developments from a reversible solid behavior to irreversible solid behavior.

The PMF-approach is first presented and then applied to some complex examples of inhomogeneous solids exhibiting texture-related toughening.

2. PMF–fracture approach for LEM

Consider a solid in its reference configuration discretized by $N = n_x n_y n_z$ mass points in the x, y and z directions on a cubic lattice of unit cell size a_0 (Fig. 1). Each mass point i (initial position $\vec{X}_i$) interacts with a fixed number of neighboring points j (18 in this paper –so-called D3Q18 lattice– corresponding to a cut-off radius $r_{cut} = \sqrt{2}a_0$ used for the neighbor-list definition in PMF approaches) via the interaction potential as a function of the translational and rotational degrees of

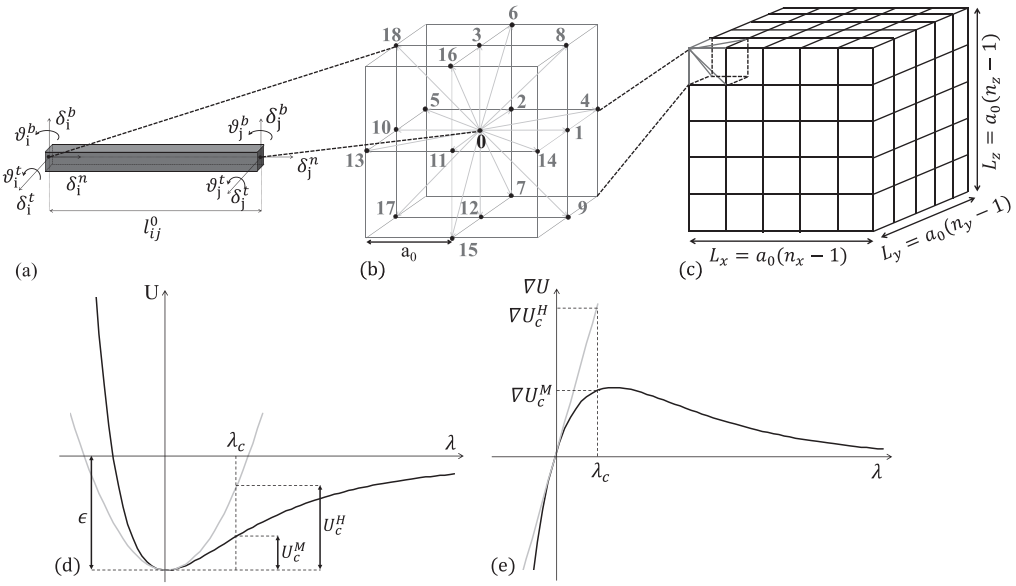

Fig. 1. (a) Degrees of freedom of a bond element between points i and j, (b) D3Q18 unit cell, (c) simulation box, (d) harmonic (gray curves) and Morse (black curves) interaction potentials and (e) associated gradient (i.e. force/moment).

freedom of the two mass points ($\vec{\delta}_i = \vec{x}_i - \vec{X}_i, \vec{\delta}_j = \vec{x}_j - \vec{X}_j, \vec{\vartheta}_i, \vec{\vartheta}_j$):

$$U_{ij} = U_{ij}^s + U_{ij}^b \,, \tag{1}$$

where $U_{ij}^s = U_{ij}^s\left(\delta_j^n - \delta_i^n\right)$ defines the two-body 'stretch' interactions in function of the change in distance between mass points i and j; with $\delta_i^n = \vec{\delta}_i \cdot \vec{e}_n^{\,ij}$ and $\delta_j^n = \vec{\delta}_j \cdot \vec{e}_n^{\,ij}$ the displacement components in the bond direction $\vec{e}_n^{\,ij} = \vec{r}_{ij}/l_{ij}^0$ [with $\vec{r}_{ij} = \vec{X}_j - \vec{X}_i = l_{ij}^0 \vec{e}_n^{\,ij}$ the vector connecting node i to node j of rest-length $l_{ij}^0 = \alpha a_0$ ($\alpha = 1$ for bonds parallel to the cubic lattice directions; and $\alpha = \sqrt{2}$ for diagonal bonds), oriented by unit vector $\vec{e}_n^{\,ij}$ in a local orthonormal basis $(\vec{e}_n, \vec{e}_b, \vec{e}_t)^{ij}$]; whereas $U_{ij}^b = U_{ij}^b\left(\vec{\vartheta}_j - \vec{\vartheta}_i; \delta_j^b - \delta_i^b; \delta_j^t - \delta_i^t\right)$ considers bending interaction terms associated with rotations, $\vec{\vartheta}_j - \vec{\vartheta}_i$, and transversal displacements, $\delta_j^b - \delta_i^b = (\vec{\delta}_j - \vec{\delta}_i) \cdot \vec{e}_b^{\,ij}$ and $\delta_j^t - \delta_i^t = (\vec{\delta}_j - \vec{\delta}_i) \cdot \vec{e}_t^{\,ij}$ in a local right-handed orthonormal basis associated to bond ij. With this parameterization, the interaction forces and moments between two mass points i and j that derive from the effective potential U_{ij} satisfy force and moment equilibrium, that is (for a detailed derivation, see Laubie et al., 2017b):

$$\vec{F}_i^{\,j} = -\frac{\partial U_{ij}}{\partial \vec{\delta}_i}; \quad \vec{F}_i^{\,j} + \vec{F}_j^{\,i} = \vec{0} \,, \tag{2}$$

$$\vec{M}_i^{\,j} = -\frac{\partial U_{ij}}{\partial \vec{\vartheta}_i}; \quad \vec{M}_i^{\,j} + \vec{M}_j^{\,i} + \vec{r}_{ij} \times \vec{F}_j^{\,i} = \vec{0} \,. \tag{3}$$

After prescribing a mechanical load (force or displacement) to the lattice structure, the relaxed configuration is obtained by minimizing the potential energy. For the purpose of this study, a non-linear conjugate gradient method was used for the numerical energy minimization: the Fletcher–Reeves–Polak–Ribiere method. For such discrete system, the stresses are modeled using the virial expression; while neglecting the momentum term (Christoffersen et al., 1981):

$$\boldsymbol{\sigma}_i = \frac{1}{2V_i} \sum_{j=1}^{N_i^b} \vec{r}_{ij} \otimes \vec{F}_i^{\,j} \,, \tag{4}$$

with V_i denoting the volume of the unit cell, and N_i^b representing the number of node i's neighboring mass points. The stress in volume V composed of N mass points is simply the volume average of the local stresses; that is:

$$\langle \boldsymbol{\sigma} \rangle = \frac{1}{V} \sum_{i=1}^{N} V_i \boldsymbol{\sigma}_i \,. \tag{5}$$

All what it takes to implement the LEM approach is to choose appropriate expressions for the interaction potential representative of the solid's behavior. This has been illustrated by Laubie et al. (2017b) for elastic isotropic and transversely

isotropic solids; and by Monfared et al. (2017) for linear poroelastic systems. The focus of the next sections is to extend the PMF approach to fracture problems.

2.1. Local approach to LEM fracture mechanics

Classical approaches to fracture problems using LEM are generally based on strength criteria that restrict the admissible values of the forces and moments $(\vec{F}_i^j, \vec{M}_i^j)$ to a threshold value beyond which the bond ij is considered as broken; hence:

$$f\left(\vec{F}_i^j,\ \vec{M}_i^j\right) \leq 0. \tag{6}$$

In contrast, in fracture mechanics, an appropriate local fracture criterion should be based on an energy criterion. If one considers that the energy dissipated when the bond breaks equals the energy stored in the bond between the equilibrium state, $r_0 = l_{ij}^0$, and the critical state, $r_c = l_{ij}^0(1+\lambda_c)$, an appropriate local fracture criterion is of the form:

$$\forall ij;\ \begin{cases} \Delta U_{ij} = U_{ij}\left(r_{ij}\right) - U_{ij}\left(l_{ij}^0\right) \leq U_{ij}(r_c) - U_{ij}(r_0) = \mathcal{G}_c^b d\Gamma_{ij} \\ d\Gamma_{ij} \geq 0 \\ \left(\Delta U_{ij} - \mathcal{G}_c^b d\Gamma_{ij}\right) d\Gamma_{ij} = 0 \end{cases} \tag{7}$$

where $\mathcal{G}_c^b = \left(U_{ij}(r_c) - U_{ij}(r_0)\right)/d\Gamma_{ij}$ can be considered as the bond's fracture energy which is dissipated in the local fracture surface creation $d\Gamma_{ij} = (\alpha a_0)^2$ situated in the plane defined by unit normal $\vec{e}_n^{\,ij}$.

2.1.1. Central–force PMF fracture approach

To illustrate this fracture criterion, we first focus on central-force lattices, in which interactions are solely defined by the stretch energy $U_{ij} = U_{ij}^s\left(\delta_j^n - \delta_i^n = \lambda_{ij}^n l_{ij}^0\right)$. In the isotropic elastic case, such central-force cubic lattices are well known to restrict the domain of application to solids exhibiting a Poisson's ratio $\nu = 1/(D+1)$ (with D the space dimension) (see e.g., Laubie et al., 2017b). With a focus on linear and non-linear fracture mechanics, consider, for purpose of illustration of the PMF-approach, the Morse potential (Morse, 1929):

$$U_{ij}^M = -\epsilon_{ij}^0 + \frac{\epsilon_{ij}^n}{2\beta^2}\left\{1 - \exp\left(-\beta\lambda_{ij}^n\right)\right\}^2, \tag{8}$$

with $\beta = \sqrt{\epsilon_{ij}^n/(2\epsilon_{ij}^0)}$ (to ensure that $U_{ij}^M \to 0$ for $\lambda_{ij}^n \to +\infty$) and the associated bond force according to Eq. (2):

$$F_j^{i,n} = \frac{\epsilon_{ij}^n}{\beta l_{ij}^0}\exp\left(-\beta\lambda_{ij}^n\right)\left\{\exp\left(-\beta\lambda_{ij}^n\right) - 1\right\}, \tag{9}$$

or equivalently, replacing the linear dilation (or stretch) in the bond direction $\lambda_{ij}^n = \left(\delta_j^n - \delta_i^n\right)/l_{ij}^0$ by the Morse potential:

$$F_j^{i,n} = \frac{\epsilon_{ij}^n}{\beta l_{ij}^0}\left\{1 + \frac{U_{ij}^M\left(\lambda_{ij}^n\right)}{\epsilon_{ij}^0} + \text{sign}\,(\lambda)\left(1 + \frac{U_{ij}^M\left(\lambda_{ij}^n\right)}{\epsilon_{ij}^0}\right)^{1/2}\right\}. \tag{10}$$

Herein, $-\epsilon_{ij}^0$ defines the well-depth at rest length $r_0 = l_{ij}^0$; while β governs the elastic response. Furthermore, a Taylor expansion of U_{ij}^M around the equilibrium position for $\lambda_{ij}^n \ll 1$ shows that the Morse potential degenerates to a harmonic potential:

$$U_{ij}^M = U_{ij}^{H,s}(\lambda_{ij}) + O\left(\left(\lambda_{ij}^n\right)^3\right), \tag{11}$$

with:

$$U_{ij}^H(\lambda_{ij}) = -\epsilon_{ij}^0 + \frac{\epsilon_{ij}^n}{2}\left(\lambda_{ij}^n\right)^2. \tag{12}$$

Such a harmonic potential expression is akin to classical truss theory employed in central-force LEM formulations in 2-D (Hansen et al., 1989; Topin et al., 2007) and 3-D (Affes et al., 2012; Kosteski et al., 2012; Nayfeh and Hefzy, 1978). In its turn, the energy parameter ϵ_{ij}^n which defines the linear elastic behavior around the equilibrium position is defined by the elasticity of the solid; for instance for an isotropic material defined by Young's modulus E and Poisson's ratio ν:

$$\epsilon_{ij}^n = E a_0^3 \mathcal{F}_n(\nu), \tag{13}$$

where the dimensionless function $\mathcal{F}_n(\nu)$ is defined for each bond direction, and takes into account the solid's Poisson ratio, ν, and the level of discretization n of the solid (for a detailed derivation, and extension to transverse isotropy, see Laubie et al., 2017b).

For the Morse potential thus defined, use of the critical energy criterion (7) in the force expression (10) provides a means to determine the maximum admissible force in the form:

$$\forall ij;\ \begin{cases} F_j^{i,n}\left(\lambda_{ij}^n\right) \le F_j^{i,n}(\lambda_c) \\ d\Gamma_{ij} \ge 0 \\ \left(F_j^{i,n}\left(\lambda_{ij}^n\right) - F_j^{i,n}(\lambda_c)\right) d\Gamma_{ij} = 0 \end{cases}, \tag{14}$$

with (noting that $U_{ij}^M(\lambda_c) = \mathcal{G}_c^b d\Gamma_{ij} - \epsilon_{ij}^0$):

$$F_j^{i,n}(\lambda_c) = a_0\left(2\alpha\beta\mathcal{G}_c^b + \text{sign}(\lambda)\mathcal{K}_c\sqrt{a_0}\right), \tag{15}$$

with:

$$\mathcal{K}_c = K_{Ic}^b\sqrt{2\mathcal{F}_n(\nu)}\,. \tag{16}$$

By analogy with Linear Elastic Fracture Mechanics (LEFM) and Irwin's formula (Irwin, 1958), $K_{Ic}^b = \sqrt{\mathcal{G}_c^b\, E}$ can be viewed as a local fracture toughness. In fact, an almost classical toughness criterion is recovered for the linear case, when considering the harmonic expression of the interaction potential (12); that is, when noting $\mathcal{G}_c^b d\Gamma_{ij} = U_{ij}^H(\lambda_c) + \epsilon_{ij}^0 = \frac{1}{2}\epsilon_{ij}^n\lambda_c^2$,

$$F_i^{j,n}\left(\lambda_c = \sqrt{\frac{2\mathcal{G}_c^b d\Gamma_{ij}}{\epsilon_{ij}^n}}\right) = \mathcal{K}_c a_0\sqrt{a_0}\,. \tag{17}$$

Otherwise said, classical strength-based approaches of LEM can be employed provided that the local strength associated with bond rupture considers the appropriate scaling with the lattice size according to Eqs. (17) and (15) for the LEFM case and the non-linear fracture mechanics case, respectively. The difference between linear and non-linear fracture mechanics using the PMF-inspired LEM-fracture approach is sketched in Fig. 1(d) and (e).

2.1.2. Consideration of bending interaction potentials

Considering a bending interaction potential U_{ij}^b –in addition to a stretch term U_{ij}^s– permits extending the realm of the LEM method on cubic lattices, in the isotropic case, to lower Poisson's ratios that the limit value defined by the central-force method, $\nu \le \nu_{\text{lim}} = 1/(D+1)$; and similar restrictions apply to transversely isotropic elastic materials (see Laubie et al., 2017b). Such limitations could be overcome by introducing a non-local term to these stretch and bending interactions (Chen et al., 2014). As far as local fracture criteria are concerned, the approach developed here above remains valid, when considering in the local fracture energy criterion (7) the bending term. To illustrate our purpose, we restrict ourselves to the hypothetical case of pure three-point bending interactions, $U_{ij} = -\epsilon_{ij}^0 + U_{ij}^b\left(\vec{\vartheta}_j - \vec{\vartheta}_i; \delta_j^b - \delta_i^b; \delta_j^t - \delta_i^t\right)$, with U_{ij}^b given –for small rotations $||\vec{\vartheta}_i|| \ll 1$ and neglecting torsional terms– by the harmonic expression:

$$\begin{aligned} U_{ij}^b = \frac{1}{2}\epsilon_{ij}^t\Big\{ &\left(\Delta_\delta^b - \vartheta_i^t\right)^2 + \left(\Delta_\delta^t + \vartheta_i^b\right)^2 \\ &-\left(\Delta_\delta^b - \vartheta_i^t\right)\Delta_\vartheta^t + \left(\Delta_\delta^t + \vartheta_i^b\right)\Delta_\vartheta^b \\ &+\frac{1}{3}\left(\left(\Delta_\vartheta^b\right)^2 + \left(\Delta_\vartheta^t\right)^2\right)\Big\}\,, \end{aligned} \tag{18}$$

with $\Delta_\vartheta^{b,t} = \vartheta_j^{b,t} - \vartheta_i^{b,t}$ and $\Delta_\delta^{b,t} = \left(\delta_j^{b,t} - \delta_i^{b,t}\right)/l_{ij}^0$. Herein, ϵ_{ij}^t is the transverse energy parameter governing the three-body interaction; analogous to beam bending terms employed in classical beam-type inspired LEM approaches (in the form $\epsilon_{ij}^t = 12E_bI/l_{ij}^0$ with E_b and I the beam's Young's modulus and second-order area moment, respectively, Bolander Jr and Saito, 1998; Schlangen and Garboczi, 1996; 1997), which gives rise to shear forces and bending moments; namely:

$$\begin{cases} \vec{F}_i^j = -\frac{\partial U_{ij}^b}{\partial\vec{\delta}_i} = \underbrace{\frac{\epsilon_{ij}^t}{l_{ij}^0}\left(\Delta_\delta^b - \vartheta_i^t - \frac{1}{2}\Delta_\vartheta^t\right)\vec{e}_b}_{F_i^{j,b}} + \underbrace{\frac{\epsilon_{ij}^t}{l_{ij}^0}\left(\Delta_\delta^t + \vartheta_i^b + \frac{1}{2}\Delta_\vartheta^b\right)\vec{e}_t}_{F_i^{j,t}} \\ \vec{M}_i^j = -\frac{\partial U_{ij}^b}{\partial\vec{\vartheta}_i} = \underbrace{-\frac{\epsilon_{ij}^t}{2}\left(\Delta_\delta^t + \vartheta_i^b + \frac{1}{3}\Delta_\vartheta^b\right)\vec{e}_b}_{M_i^{j,b}} + \underbrace{\frac{\epsilon_{ij}^t}{2}\left(\Delta_\delta^b - \vartheta_i^t - \frac{1}{3}\Delta_\vartheta^t\right)\vec{e}_t}_{M_i^{j,t}} \end{cases}. \tag{19}$$

By inverting this linear system, and substituting the results into the bending energy expression (18), one obtains after some transformations with the help of (3):

$$U_{ij}^b = \frac{2}{\epsilon_{ij}^t}\left(\left|\left|\vec{M}_i^j\right|\right|^2 + \left|\left|\vec{M}_j^i\right|\right|^2 - \vec{M}_i^j\cdot\vec{M}_j^i\right). \tag{20}$$

Finally, use of this expression in the local fracture energy criterion (7) –while noting that $\Delta U_{ij} = U_{ij}^b$ – provides a local-force-moment strength criterion:

$$\left\{4\frac{\epsilon_{ij}^n}{\epsilon_{ij}^t}\left(\left|\left|\vec{M}_i^j\right|\right|^2 + \left|\left|\vec{M}_j^i\right|\right|^2 - \vec{M}_i^j \cdot \vec{M}_j^i\right)\right\}^{1/2} \leq \mathcal{K}_c a_0 \sqrt{a_0}\,, \tag{21}$$

where toughness $\mathcal{K}_c$ is defined by (16).

Finally, if both stretch and bending terms are considered, a straightforward analogous development provides for the harmonic case the local force–moment fracture criterion:

$$\text{sign}\left(F_j^{i,n}\right)\left\{\left(F_j^{i,n}\right)^2 + 4\frac{\epsilon_{ij}^n}{\epsilon_{ij}^t}\left(\left|\left|\vec{M}_i^j\right|\right|^2 + \left|\left|\vec{M}_j^i\right|\right|^2 - \vec{M}_i^j \cdot \vec{M}_j^i\right)\right\}^{1/2} \leq \mathcal{K}_c a_0 \sqrt{a_0}\,, \tag{22}$$

with $\text{sign}\left(F_i^{j,n}\right)$ accounting for the fact that fracture only occurs when bond elements are in tension.

These local force criteria are readily implemented in existing LEM approaches that employ strength-based criteria for bond removals (resulting in crack initiation and/or propagation) (Affes et al., 2012; Bolander Jr and Saito, 1998; Chiaia et al., 1997; Hansen et al., 1989; Lilliu and van Mier, 2003; van Mier, 1996; Mohammadipour and Willam, 2015; 2016; Schlangen and Garboczi, 1996; 1997; Topin et al., 2007; van Mier et al., 2002). That is, for a given load, after energy minimization, all bonds of forces and moments greater than the threshold value are removed. The sole difference with existing approaches is the scaling of this force threshold value with $\mathcal{K}_c a_0 \sqrt{a_0}$.

2.2. Global approach to LEM fracture mechanics

In contrast to the local approach, one could equally follow Griffith's global approach (Griffith, 1921). Under quasi-static conditions, the approach consists of considering fracture as a sequence of relaxed equilibrium states at constant loading, with the change in potential energy attributed to spontaneous energy changes related to dissipation by fracture surface creation. Adopting the Griffith approach for the PMF-inspired LEM-approach, fracture is viewed as a release of the bond energy at lattice sites, which is achieved by removing one mass point i among the N mass points of the system. The potential energy of the system before and after mass point removal is considered to realize a minimum; that is, before fracture propagation in a displacement-driven fracture test:

$$\delta\mathcal{E}_{pot}^N = U^N - U_0^N = \min_{(\vec{\delta}_k, \vec{v}_k)} \frac{1}{2}\sum_{i=1}^{N}\sum_{j=1}^{N_i^b}\left(U_{ij}^- + \epsilon_{ij}^0\right)\,, \tag{23}$$

and after fracture propagation:

$$\delta\mathcal{E}_{pot}^{N-1} = U^{N-1} - U_0^{N-1} = \min_{(\vec{\delta}_k, \vec{v}_k)} \frac{1}{2}\sum_{i=1}^{N-1}\sum_{j=1}^{N_i^b}\left(U_{ij}^+ + \epsilon_{ij}^0\right)\,, \tag{24}$$

where U_{ij}^- and U_{ij}^+ stand for the values of the relaxed local interaction potentials before and after mass point removal at a fixed prescribed displacement. The fracture created by the removal of one mass point on a regular cubic lattice is $d\Gamma(\zeta a_0)^2$, where $\zeta = 1$ if the mass point removed is connected to an existing fracture[1], and $\zeta = 2$ otherwise. Following Griffith's approach, the change of the potential energy due to fracture, $\Delta\mathcal{E}_{pot} = \delta\mathcal{E}_{pot}^{N-1} - \delta\mathcal{E}_{pot}^N$, occurs spontaneously, that is, at constant loading, when the energy release rate, $\mathcal{G}$, reaches a threshold, the material's fracture energy $\mathcal{G}_c$; that is:

$$\mathcal{G} = -\frac{\partial\mathcal{E}_{pot}}{\partial\Gamma} \simeq -\frac{\Delta\mathcal{E}_{pot}}{d\Gamma} \leq \mathcal{G}_c\,. \tag{25}$$

When $\mathcal{G} = \mathcal{G}_c$, the fracture occurs and dissipates an energy dD:

$$dD = \mathcal{G}d\Gamma \overset{\mathcal{G}=\mathcal{G}_c}{=} \mathcal{G}_c(\zeta a_0)^2 \geq 0\,. \tag{26}$$

Evoking the principle of non-economy of matter, we thus need to search for the mass point $k_{\max} \in \{1, \ldots, N\}$, whose removal entails the greatest energy dissipation; that is:

$$k_{max} = \text{argmax}_k \mathcal{G}(k) \geq \mathcal{G}_c;\;\; \mathcal{G}(k) = \frac{\left(\delta\mathcal{E}_{pot}^N - \delta\mathcal{E}_{pot}^{N-1}(k)\right)}{(\zeta a_0)^2}\,, \tag{27}$$

with $\delta\mathcal{E}_{pot}^{N-1}(k)$ the potential energy associated with the removal of the kth mass-point. The global fracture criterion reads as:

$$\mathcal{G} \leq \mathcal{G}_c;\;\; d\Gamma \geq 0;\;\; (\mathcal{G} - \mathcal{G}_c)d\Gamma = 0\,. \tag{28}$$

[1] In that case, all the bonds crossing the new crack plane are also removed.

Thus, from Eq. (27) it is readily understood that the approach will favor mass point removal adjacent to existing cracks ($\zeta = 1$), which simplifies the algorithmic implementation of the global fracture criterion. If an initial crack exists, only nodes surrounding the initial crack-tip are considered in (27)), otherwise all the nodes need to be considered. In this case, failure is expected to be triggered in regions of high local stress due to local defects or heterogeneities. In contrast to the local approach, the drawback of the global approach is that it requires, for a given load, N_k–energy minimization steps, with N_k the number of mass points to be removed to satisfy the global fracture criterion (28). This makes the global approach computationally less efficient than the local fracture-strength approach.

On the other hand, from a PMF-perspective, the global fracture energy approach using LEM has much in common with Grand Canonical ensemble (μVT) Monte Carlo (GCMC, with μ the chemical potential) simulation techniques that are available in many molecular simulation platforms, and which may speed up the search for the maximum energy dissipation according to Eq. (27). In GCMC (see Appendix for more details), the acceptance criteria show that if the energy difference ΔU is such that$\Delta U > \mu$, there is a higher probability of accepting a mass point insertion, while for $\Delta U < -\mu$ or $-\Delta U > \mu$ mass point deletion is favored. Thus, for a given value of ΔU associated with mass point insertion or deletion, one can search for the value of the chemical potential, μ, that produces mass insertion or deletion. Applied to a displacement-controlled fracture propagation, for which $U = \mathcal{E}_{pot}$, one evaluates the potential energy, at constant prescribed displacement (u^d), before ($\mathcal{E}^N_{pot}$) and after mass point insertion ($\mathcal{E}^{N+1}_{pot}$) or deletion ($\mathcal{E}^{N-1}_{pot}$). Hence, if $-\Delta U = \left(\mathcal{E}^N_{pot} - \mathcal{E}^{N-1}_{pot}\right)_{u^d} > \mu$, it is more likely that the deletion move is accepted, whereas it is unlikely that $\Delta U = \left(\mathcal{E}^{N+1}_{pot} - \mathcal{E}^N_{pot}\right)_{u^d} > \mu$. That is, using a GCMC-approach, it becomes possible to identify, for a given value of the chemical potential μ, the total number $N_{tot} \ll N$ of mass points that need to be removed until $-\Delta U = -\Delta\mathcal{E}_{pot} = \mu$. This 'equilibrium' condition[2] corresponds precisely to the fracture criterion (25), and allows us to identify for this converged GCMC simulation:

$$\mu = \mathcal{G}_c^{N_{tot}}\ k(\zeta a_0)^2 + \Delta U_0\ , \tag{29}$$

where $\mathcal{G}_c^{N_{tot}}$ is the fracture energy released in the creation of the fracture surface $k(\zeta a_0)^2$, whereas $\Delta U_0 = U_0^{N-k} - U_0^N$ is the ground state energy of the N_{tot} deleted mass points:

$$\Delta U_0 = \sum_{i=1}^{N_{tot}} \sum_{j=1}^{N_i^b} \epsilon_{ij}^0 \geq 0\ . \tag{30}$$

This comforts the idea that the global Griffith approach is but an analogous GCMC approach suitable for fracture propagation simulations. In this approach, the mass point removal can be seen as a lattice erosion, with the number of removed mass points that is much smaller than the total number of points in the simulation box. The total mass is thus conserved although the removed mass is no more connected to the rest of the lattice.

3. Verification: fracture propagation in homogeneous media

The two approaches, local vs. global, thus suggested differ fundamentally in their theoretical basis and algorithmic implementation. Their coexistence thus requires to show the duality of the two approaches. This is the focus of this verification section which applies both approaches to fracture propagation in homogeneous media.

As reference problem, consider a 2-D plane-stress square plate of size $L = L_x = L_z = (n-1)a_0$ ($n_x = n_z = n$) and thickness a_0 ($n_y = 2$), with an edge crack of length $l_0 = L/5$ (Fig. 2). The system is subject to a pure Mode I displacement loading in form of a triangular displacement at the top and bottom surfaces of the sample, with a maximum displacement $\delta/2$ applied at the edges above and below the notch. The toughness of the different brittle solids investigated was chosen such that the lattice deformations remain small throughout the loading process.

3.1. Calibration

Considering a discretization by n mass points of unit cell-size a_0 on a regular 2-D cubic lattice, the parameterization of the energy parameters for isotropic solids by (Laubie et al., 2017b, Table 2) is employed; that is, for bonds parallel to the box boundaries (rest-length $l_{ij}^0 = a_0$), and for diagonal bonds (rest-length $l_{ij}^0 = \sqrt{2}a_0$) of the D3Q18–lattice:

$$\begin{cases} \epsilon_{ij}^n\left(l_{ij}^0 = a_0\right) &= \frac{n(2-3\nu)-2(1-\nu)}{4n\left(1-\nu^2\right)} E a_0^3 \\ \epsilon_{ij}^n\left(l_{ij}^0 = \sqrt{2}a_0\right) &= \frac{\nu}{\left(1-\nu^2\right)} E a_0^3 \\ \epsilon_{ij}^t\left(l_{ij}^0 = a_0\right) &= \frac{(n-1)(1-3\nu)}{2n\left(1-\nu^2\right)} E a_0^3 \end{cases}, \tag{31}$$

where E is the solid's Young's modulus, and ν the Poisson's ratio situated within the limits, $0 \leq \nu \leq 1/3$ for the 2-D system considered. For purpose of comparison of the local and global approach, we consider $\nu = 1/3$, so that bending interactions

[2] It should be noted that the equilibrium condition, $-\Delta U = -\Delta\mathcal{E}_{pot} = \mu$, in the GCMC-approach is an ensemble average, as the simulations will exhibit fluctuations between insertion and deletion of a mass point.

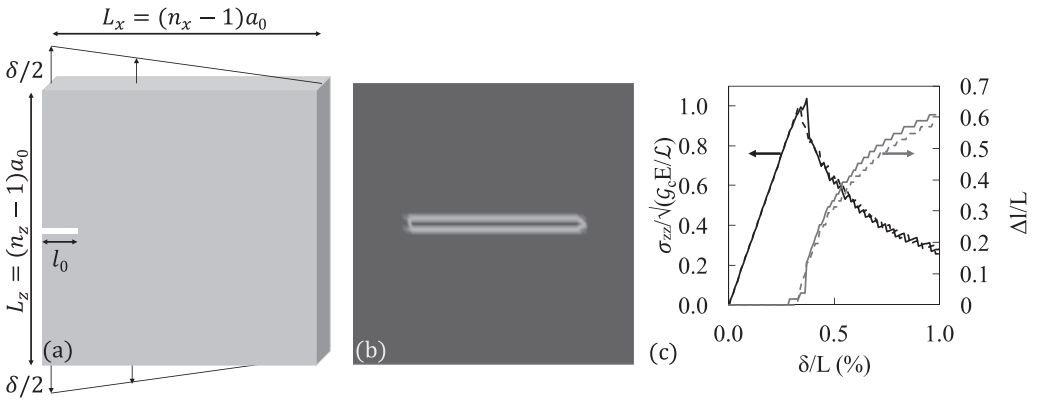

Fig. 2. (a) Mode I loading of a quasi-2D square plate, (b) simulation box after crack propagation with the region where bonds were broken highlighted and (c) left axis (black curves): stress-strain curves obtained using the global approach in LEM (dashed line) and the local approach (solid line) ($n = 51$), right axis (gray curves): evolution of the crack length extension $\Delta l/L$ using the global approach (dashed line) and the local approach (solid line). The stress is normalized by $\sqrt{\mathcal{G}_c E/\mathcal{L}}$ with $\mathcal{L} \sim l_0$.

are neglected ($\epsilon_{ij}^t = 0$). Considering in addition harmonic potentials, the local fracture criterion is given by Eq. (14) with the force threshold defined by Eqs. (16) and (17):

$$F_i^{j,n} \leq f_c = \mathcal{K}_c\left(l_{ij}^0\right) a_0^{3/2} = K_{Ic}^b a_0^{3/2} \begin{cases} \frac{3}{4}\sqrt{\frac{1}{n}\left(n - \frac{4}{3}\right)} & \text{if:} \quad l_{ij}^0 = a_0 \\ \sqrt{\frac{3}{4}} & \text{if:} \quad l_{ij}^0 = \sqrt{2}a_0 \end{cases}, \tag{32}$$

where $K_{Ic}^b = \sqrt{\mathcal{G}_c^b E}$ is the bond's fracture toughness. It was found after a post-mortem analysis of the simulation boxes that on average 10 bonds break for one crack advance, resulting in $\mathcal{G}_c = \kappa \mathcal{G}_c^b$ with $\kappa \simeq 10$ and $\mathcal{G}_c$ the material's fracture energy. The bond's fracture toughness K_{Ic}^b can thus be calibrated against the solid's fracture energy: $K_{Ic}^b = \sqrt{\kappa \mathcal{G}_c E}$ or the solid's fracture toughness, K_{Ic}: $K_{Ic}^b = \sqrt{\kappa} K_{Ic}$. This value of κ depends on the geometry of the background lattice. The value given here reflects the connectivity of the D3Q18 lattice only.

3.2. Stress–strain response and scaling

The focus of the validation is to show that the local and the global LEM-fracture approaches are consistent with linear elastic fracture mechanics theory. This is achieved here by inspecting the average stress-strain response (stress $\langle \sigma_{zz} \rangle = \vec{e}_z \cdot \langle \boldsymbol{\sigma} \rangle \cdot \vec{e}_z$ vs. δ/L) in the direction of load application for different discretization levels ($n = 1 + L/a_0 = 25$, 51 and 101) for both the global and the local approach, as displayed in Fig. 3 (a) and (b), respectively. The results indicate (1) an identical stress-strain response for different levels of discretization n, when $(E, \mathcal{G}_c)$ in the global approach, and (E, K_{Ic}) in the local approach are maintained constant; (2) a linear scaling of the average peak-stress σ^c with $\sqrt{\mathcal{G}_c E}$ in the global approach when varying $\mathcal{G}_c$ and E; (3) a linear scaling of the average peak-stress with K_{Ic} in the local approach, independently of the stiffness E. These stress-strain responses confirm the relevant feature of LEFM: $\sigma^c \sim K_{Ic}\sqrt{l_0}$ (see e.g. Sun and Jin, 2012) predicted by the PMF-inspired global and local fracture approach with harmonic potentials. The good comparison of the two approaches also evidences the duality of the local and global approach (Fig. 2 (c)).

3.3. Duality of local and global approaches

Further evidence of the duality of the two approaches is provided here by comparing the energy release rates predicted respectively by the global and the local approach. To this end, the energy release rate is evaluated using the $J-$integral or Rice-integral (Rice, 1968):

$$\mathcal{G} = J = \int_C \left(\psi \left(\vec{e}_1 \cdot \vec{n} \right) - \frac{\partial \vec{u}}{\partial x_1} \cdot \vec{T} \right) ds \,, \tag{33}$$

where ψ is the free energy volume density, $\vec{u}$ the displacement, $\vec{T}(\vec{n})$ the stress vector along the closed contour C (of unit normal vector $\vec{n}$) which includes the crack oriented in the $\vec{e}_1$ direction. For the problem at hand, the sole contribution to the J-integral comes from the top and bottom boundaries oriented by $\vec{n} = \pm \vec{e}_z$, for which $\partial \vec{u}/\partial x_1 = \mp \delta/(2L)\ \vec{e}_z$, and hence:

$$\mathcal{G} = J = \frac{\delta}{L} \int_{x=0}^{L} \sigma_{zz} dx = \delta \langle \sigma_{zz} \rangle \,, \tag{34}$$

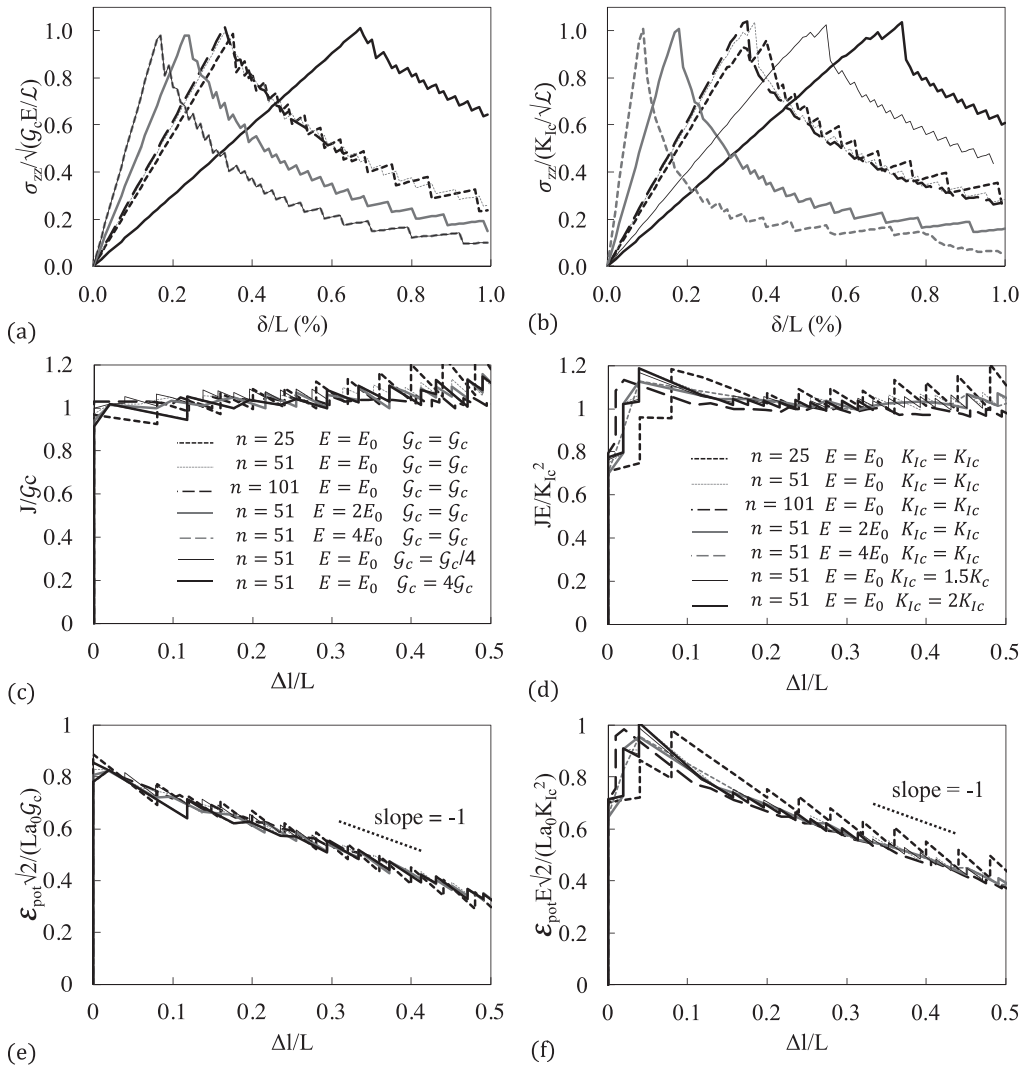

Fig. 3. (a) and (b) Stress-load curves obtained using the global approach and the local approach, respectively (stress normalized by $\sqrt{\mathcal{G}_c E/\mathcal{L}}$ or $K_{Ic}/\sqrt{\mathcal{L}}$ with $\mathcal{L} \sim l_0$). (c) and (d) Dimensionless J-integral as function of the dimensionless crack length extension $\Delta l/L$ using the global approach and the local approach, respectively. (e) and (f) Dimensionless potential energy as function of the dimensionless crack length extension $\Delta l/L$ using the global approach and the local approach, respectively. LEM simulations for different discretizations (n), stiffnesses (E) and fracture energies $\mathcal{G}_c$ or toughnesses K_{Ic}, legend on (c) (and, (d)) holds for (a) and (e)(and, (b) and (f)).

with $\langle \sigma_{zz} \rangle$ evaluated from the virial stress expression, $\langle \sigma_{zz} \rangle = \vec{e}_z \cdot \langle \boldsymbol{\sigma} \rangle \cdot \vec{e}_z$. Fig. 3 (c) and (d) show the evolution of the energy release rate ($\mathcal{G} = J$) vs. the crack length extension ($\Delta l = l - l_0$) in a normalized plot. After the elastic loading phase (no crack propagation), the dimensionless energy release rate ($J/\mathcal{G}_c$ in the global approach, and JE/K_c^2 in the local approach) rapidly converges to 1; independent of the discretization (n), the stiffness (E) and the value of the fracture energy or fracture toughness, related by Irwin's formula $K_{Ic} = \sqrt{E\mathcal{G}_c}$. While a finer discretization (i.e. an increase in the number of mass points per side corresponding to a decrease in a_0) smooths the J vs $\Delta l/L$ curves, the (almost) perfect agreement between the local and the global approach confirms the duality of the two approaches.

One could argue that the $J-$integral evaluation of the energy release rate $\mathcal{G}$ is biased by the use of an averaged stress quantity, and not by a direct measurement of the (spontaneous) change in potential energy due to fracture. To address this question we calculate the actual potential energy obtained for each load step. In order for the energy release to be constant and equal to the fracture energy, $\mathcal{G} = \mathcal{G}_c$, in this displacement controlled fracture test, the potential energy, according to its continuum definition, $\mathcal{G} = -\partial \mathcal{E}_{pot}/\partial \Gamma$, should decrease linearly with the crack length, and hence,

$$\mathcal{E}_{pot} \sim -\mathcal{G}_c d\Gamma = -\mathcal{G}_c \Delta l \left(a_0/\sqrt{n_y}\right) , \tag{35}$$

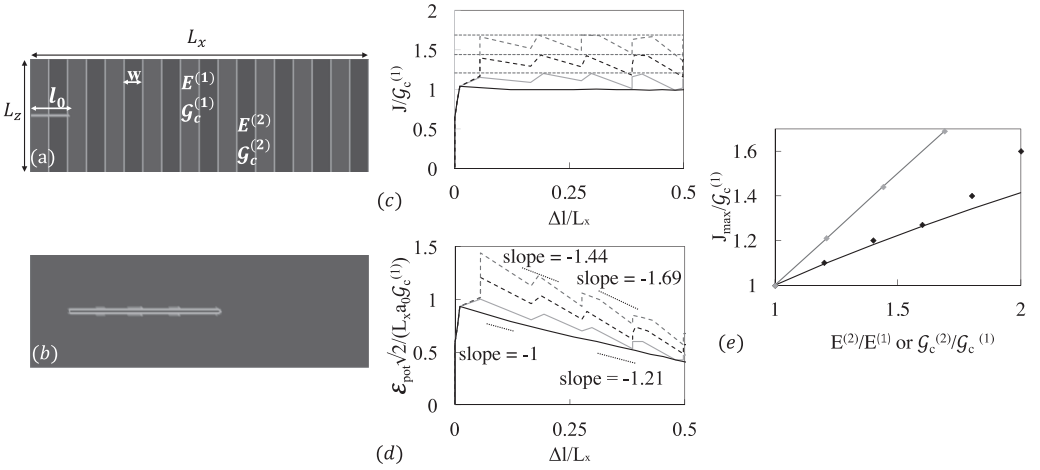

Fig. 4. (a) Geometry and parameters definition. (b) Simulation box after crack propagation (regions where bonds were broken are highlighted). Dimensionless J-integral J/G_{c1} (c) and potential energy $\mathcal{E}_{pot}\sqrt{2}/(a_0 L_x G'_{c1})$ (d) as function of the dimensionless crack length extension ($\Delta l/L_x$) for $E_1 = E_2$ and $G_{c2} = G_{c1}$ (black line), $G_{c2} = 1.21G_{c1}$ (gray line), $G_{c2} = 1.44G_{c1}$ (dashed black line) or $G_{c2} = 1.69G_{c1}$ (dashed gray line). (e) Dimensionless homogenized fracture energy J_{max}/G_{c1} as function of the stiffness ratio ($E^{(2)}/E^{(1)}$, black symbols) or toughness ratio ($\mathcal{G}^{(2)} = \mathcal{G}^{(1)}$, gray symbols). Black and gray lines correspond to Eqs. (41) and (39), respectively.

or in a dimensionless form:

$$\frac{\mathcal{E}_{pot}\sqrt{n_y}}{\mathcal{G}_c a_0 L} \sim -\frac{\Delta l}{L}\,, \tag{36}$$

where the factor $\sqrt{n_y}$ corrects for the crack extension in the in-plane direction, when $\mathcal{E}_{pot}$ is numerically evaluated in 3-D for an in-plane discretization, $n_y = 2$, representative of the 2-D fracture propagation problem. Fig. 3 (e) and (f) display the dimensionless potential energy expression, Eq. (36), in function of the dimensionless crack length extension $\Delta l/L$. After an elastic loading phase (potential energy built-up without crack propagation), the potential energy decreases indeed linearly with the crack-extension length, independently of discretization, stiffness, fracture energy ($\mathcal{G}_c$ in the global approach) or toughness (K_{Ic} in the local approach). This proves that the two approaches, global and local, are strictly equivalent, much akin to the duality of the local and global approach in continuum LEFM; though achieved by completely different means: namely by considering a GCMC-type mass-point removal algorithm in the global PMF-fracture approach; and by a proper scaling of the local fracture strength with $f_c \sim a_0^{3/2}$ in the local PMF-fracture approach. The advantage of the discrete approach over the continuum approach is that it permits studying fracture propagation in heterogeneous materials, as shown here below.

4. Toughening mechanisms in inhomogeneous media

For purpose of application, the PMF-fracture approach is employed for the investigation of toughening mechanisms in layered material systems, relevant in many applications ranging from stimulation techniques employed in oil- and gas-well applications (see e.g. Laubie and Ulm, 2014a; 2014b), to fracture resistance of hard tissues in bio-medical applications (see e.g. Ballarini et al., 2005).

Compared to the complexity of real-life systems, the example here considered is an idealized textbook example of a two-phase layered material of different mechanical properties, stiffness ($E^{(1)}$, $E^{(2)}$) and fracture energy $\left(\mathcal{G}_c^{(1)}, \mathcal{G}_c^{(2)}\right)$, whose behavior is assumed to be well described by harmonic potentials. The geometric lay-out is identical with the layered system studied by Hossain et al. (2014) using a variational fracture field approach (Bourdin et al., 2010) . Investigating toughening mechanisms due to elastic and toughness heterogeneity and toughening due to crack tortuosity, the results of Hossain et al. (2014) provide a benchmark for our LEM-fracture results, and a formidable example of the possibility of the PMF-inspired LEM-approach for investigation of fracture propagation in heterogeneous materials.

4.1. Materials and methods

As simulation sample, consider a 2-D plane-stress square plate of size $L_x = 180a_0$, $L_z = 60a_0$ and $L_y = a_0$, made of successive layers of width $w = 10a_0$, of different elastic and fracture properties, and a pre-existing crack of length $l_0 = L_x/9$ (Fig. 4(a)). The simulation sample is subjected to the same triangular displacement boundary condition as in the homogeneous case (Fig. 2). The energy parameters of the bonds of each layer are calibrated using Eq. (31) for materials exhibiting the same solid Poisson's ratio $\nu_1 = \nu_2 = 1/3$ (i.e. $\epsilon_{ij}^{t(1)} = \epsilon_{ij}^{t(2)} = 0$), and a discretization level n defined by the number of

mass points used to discretize the system. At the interface between the materials, the interaction energy is determined following the PMF-compliance-rule –consistently with the Hertz contact problem– which implies (see Masoero et al., 2014 for derivation):

$$\frac{2}{\epsilon_{ij}^{n(int)}} = \frac{1}{\epsilon_{ij}^{n(1)}} + \frac{1}{\epsilon_{ij}^{n(2)}} \,. \tag{37}$$

Similarly, using the local fracture approach, the calibration of the local fracture strength for each layer is given by Eq. (32), for different values of fracture toughness ($K_{Ic}^{(m)} = \sqrt{\mathcal{G}_c^{(m)} E^{(m)}}$; $m = 1, 2$). Strong bonding is enforced in the form:

$$f_c^{(int)} = \max\left(f_c^{(1)}, f_c^{(2)}\right) . \tag{38}$$

It should, however, be noted that this fracture-strength interface condition has little impact on the overall results in the example, as a weak bonding, $f_c^{(int)} = \min\left(f_c^{(1)}, f_c^{(2)}\right)$. The different materials parameters were chosen in order to discard in the simulations fracture propagation along the interface between two layers that can become energetically favorable (He and Hutchinson, 1989).

To investigate the impact of heterogeneity on the effective fracture properties of the composite material, the energy release due to fracture at the composite scale is probed in two ways previously introduced for the homogeneous case; namely via (1) the $J-$integral expression (34), and (2) the actual potential energy variation in function of the fracture length, i.e. Eq. (36). Both expressions should provide a means of evaluating the 'effective' macroscopic energy release rate. Indeed, the $J-$integral assumes a co-linear fracture propagation defined by the initial fracture orientation $\vec{e}_x$, and thus ignores local crack deflection and other deviations of the fracture path from its original orientation. Hence, the $J-$integral expression (34) is employed here as a means to evaluate the 'effective' energy release rate of the fracture propagation in an equivalent continuum composite with a straight crack. In contrast, the evaluation of the actual change of the potential energy from the local interaction energies through Eq. (36) provides a more realistic evaluation of the actual amount of energy that is dissipated by fracture generation. The comparison of the two quantities is expected to shed light on the toughening mechanisms induced by material inhomogeneity in the layered system.

4.2. Results

4.2.1. Toughening due to fracture energy heterogeneity

The impact of a heterogeneous distribution of fracture properties is investigated by considering that the two phases have the same stiffness ($E^{(1)} = E^{(2)}$) but different fracture energies ($\mathcal{G}_c^{(2)} > \mathcal{G}_c^{(1)}$), and thus a different fracture toughness, $K_c^{(2)}/K_c^{(1)} = f_c^{(2)}/f_c^{(1)} = \sqrt{\mathcal{G}_c^{(2)}/\mathcal{G}_c^{(1)}} > 1$). Fig. 4 (c) displays the effective normalized energy release rate evaluated from the $J-$integral, $J/\mathcal{G}_c^{(1)}$, in function of the normalized crack extension $\Delta l/L_x$, for different fracture energy contrast values $\gamma = \mathcal{G}_c^{(2)}/\mathcal{G}_c^{(1)} = 1,\ 1.21,\ 1.44,\ 1.69$ (obtained by imposing in the local fracture strength criteria (32), at constant stiffness, toughness values of $K_{Ic}^{(2)}/K_{Ic}^{(1)} = 1,\ 1.1,\ 1.2,\ 1.3$). Compared to the response of the homogeneous system obtained for $\gamma = 1$, the response exhibits a sequence of discrete jumps, reminiscent of a stick-slip–type propagation, with peak values that correspond exactly to $J_{\max} = \mathcal{G}_c^{(2)}$ (or $J_{\max}/\mathcal{G}_c^{(1)} = \gamma$). A closer inspection of the crack path shows that the crack remains straight (Fig. 4 (b)) for different values of γ, meaning that the jumps in $J/\mathcal{G}_c^{(1)}$ cannot be explained by crack deflection at interfaces. Instead, as noted by Hossain et al. (2014), the crack propagates through the low-fracture phase (1) and is then arrested at the interface with the *tough* material, until further loading induces enough elastic energy for the fracture to propagate through the tougher layer (2). This crack trapping at the tough interface entails an effective fracture energy, $\mathcal{G}_c^{eff}$, of the composite system that is equal to the one of the tougher material:

$$\mathcal{G}_c^{eff} = \max\left(\mathcal{G}_c^{(1)}, \mathcal{G}_c^{(2)}\right) . \tag{39}$$

That is, $\mathcal{G}_c^{eff}$ can be considered as the homogenized fracture energy of the layered system, in the sense that it is the fracture energy that would be sensed at the macroscopic scale of the composite for collinear fracture propagation. The dimensionless potential energy evolution with the fracture length displayed in Fig. 4 (d) supports this finding showing the seesaw pattern with slopes equal to $-\gamma$; that is in terms of Eq. (36):

$$\frac{\mathcal{E}_{pot}\sqrt{n_y}}{\mathcal{G}_c^{(1)} a_0 L_x} \sim -\gamma \frac{\Delta l}{L_x} \,. \tag{40}$$

Hence, despite an almost straight crack, heterogeneity in the fracture energy (at constant stiffness) itself can be considered as a toughening mechanism. A similar behavior was observed on a grid with twice as many mass points in the x and z directions.

Finally, it is noteworthy that in contrast to Hossain et al. (2014) who showed that the J-integral value oscillates between the low and the high fracture energy, the drop in J is less significant in our simulation results. This may be due to the difference in stability of the fracture process between the continuum approach employed by Hossain et al. (2014) and our

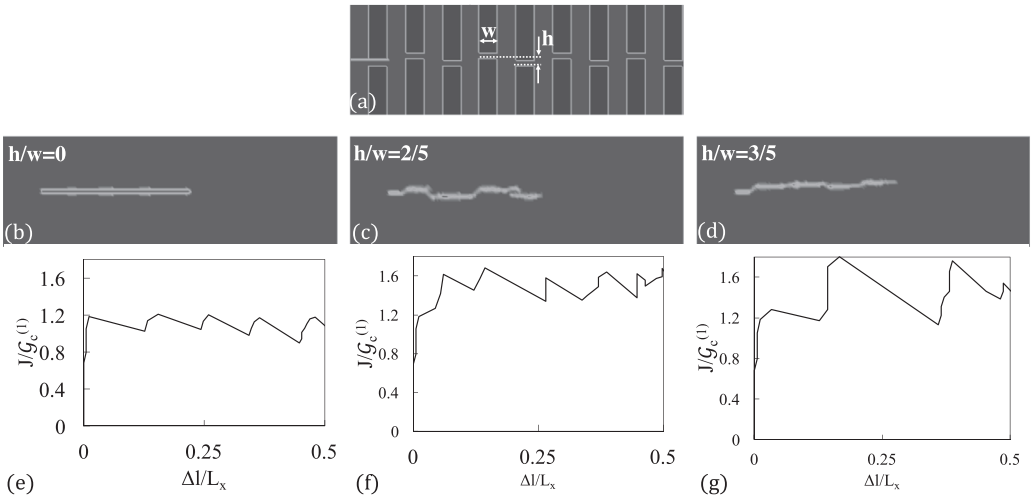

Fig. 5. (a) Geometry definition. (b)–(d) Simulation box after crack propagation. (e)–(g) Dimensionless J-integral J/G_{c1} for $h/w = 0$, 2/5 and 3/5, respectively.

discrete approach in which finite steps of energy release stabilize the fracture process in terms of potential energy minima in the quasi-static crack propagation process. This difference may also be attributed to the triangular boundary conditions used in this study as opposed to the smoother *surfing* boundary conditions used in Hossain et al. (2014).

4.2.2. Toughening due to elastic heterogeneity

The second toughening mechanism considered here is the toughening due to elastic heterogeneity ($E^{(2)} > E^{(1)}$) at same fracture energy ($\gamma = \mathcal{G}_c^{(2)}/\mathcal{G}_c^{(1)} = 1$). Since $K_{Ic}^{(m)} = \sqrt{\mathcal{G}_c E^{(m)}}$, elastic heterogeneity is readily understood to affect the local fracture strength criterion (32), that is, $f_c^{(2)}/f_c^{(1)} = \sqrt{E^{(2)}/E^{(1)}} > 1$. It is thus not surprising that the J -integral and the potential energy exhibit similar features as in the case of a fracture energy contrast, even if the fracture energy here is the same in both phases. In the range of stiffness contrast investigated here ($E^{(2)}/E^{(1)} \in [1, 2]$), the crack propagates along a straight path and gets momentarily arrested at the interface with the *stiff* phase before continuing its propagation. This gives rise to a toughening mechanism induced by elastic heterogeneity, that scales roughly as (Fig. 4 (e)):

$$\mathcal{G}_c^{(2)}/\mathcal{G}_c^{(1)} = 1; \quad \frac{\mathcal{G}_c^{eff}}{\mathcal{G}_c^{(1)}} = \frac{J_{max}}{\mathcal{G}_c^{(1)}} \simeq \left(\frac{E^{(2)}}{E^{(1)}}\right)^{1/2}. \tag{41}$$

The results are consistent with Hossain et al. (2014) findings, who suggested that toughening due to elastic heterogeneity originates from the redistribution of strain energy in the heterogeneous material. Specifically, as a crack approaches the stiff region from the compliant region, the energy that is incrementally supplied from the outside is consumed in the elastic deformation of the stiff region, before the crack continues to propagate when this energy reaches the threshold defined by the fracture energy.

4.2.3. Toughening due to crack deflection

The last toughening mechanism herein investigated relates to crack front roughening, crack deflection and crack tortuosity, that have been highlighted by several quasi-continuum approaches as a possible source of overall fracture toughening of composite materials (Faber and Evans, 1983; Gao and Rice, 1989; He and Hutchinson, 1989). Following Hossain et al. (2014), elastic heterogeneity ($E^{(2)} = 2E^{(1)}$, $\gamma = \mathcal{G}_c^{(2)}/\mathcal{G}_c^{(1)} = 1$) is paired with broken strips where the stripe of the stiff material (phase 2) has a gap through which the compliant material percolates. A misalignment (h/w) is introduced such that $h/w = 0$ for the aligned system, whereas $h/w > 0$ for gap misalignment where w stands for the strip width ($w = 10a_0$ in the simulations); see Fig. 5 (a). Given the elastic heterogeneity of the system, and the percolated compliant phase exhibiting a lower fracture toughness, $K_{Ic}^{(1)} = K_{Ic}^{(2)}/\sqrt{2}$, one would expect that the fracture would propagate along the shortest path in the compliant phase. This is indeed true for the aligned system (Fig. 5 (b); $h/w = 0$), exhibiting a straight fracture propagation associated with some small toughening, $J/\mathcal{G}_c^{(1)} > 1$, which can be attributed, for small gaps width to stress shielding by the stiffer, yet broken strips. This still holds true for moderate misalignment values (Fig. 5 (c) ; $h/w = 2/5$), for which the fracture follows indeed the shortest path through the compliant phase, up to a maximum value beyond which the crack does not deflect to remain in the soft phase, but penetrates into the stiff phase (Fig. 5 (d); $h/w = 3/5$). Misalignment thus entails a significant increase in the effective fracture energy (Fig. 5 (f) and (g)), oscillating between an upper bound defined by the elastic toughening mechanism (Eq. (41)), and a lower bound associated with crack deflection and defined by the

increase of the fracture length due to fracture tortuosity:

$$1+\frac{h}{w}\leq\frac{\mathcal{G}_c^{eff}}{\mathcal{G}_c}=\frac{J_{max}}{\mathcal{G}_c}\lessapprox\left(\frac{E^{(2)}}{E^{(1)}}\right)^{1/2}. \tag{42}$$

Otherwise said, misalignment leads to the completion of two energetically competing phenomena. As long as the crack deflection entails a higher energy dissipation than the energy release associated with propagation through the stiffer phase, misalignment will lead to toughening due to crack deflection (Fig. 5 (c)). In return, when the release of energy stored into the stiffer phase during crack arrest is greater, the crack will propagate through the stiffer phase irrespective of the gap (Fig. 5 (d)).

5. Conclusion

Fracture of heterogeneous materials is an open issue that requires a rational framework allowing for the quantification of local fracture processes with global fracture descriptors such as the energy release rate. This was the focus of the herein proposed PMF approach to discrete modeling of fracture processes using LEM:

1. Local Fracture-Strength Approach: With a focus on accounting for the actual physics interaction, the PMF-inspired LEM approach is based on effective potentials which capture the energy interaction between mass points, and from which forces and moments derive. This energy definition of interaction lends itself readily for the modeling of the rupture of bonds at a material scale, using classical fracture materials descriptors such as fracture energy and fracture toughness. It is on this basis that local fracture-strength criteria are derived, which consider the appropriate scaling commensurable with the energy dissipation of fracture processes, and according to which bonds are removed until all interaction forces and moments satisfy the local fracture-strength criterion.
2. Global Energy-Release Approach: Alternatively, the PMF-approach permits the definition of a global energy approach, by analogy with Griffith's energy release rate criterion. Considering fracture as a sequence of equilibrium states associated with minimum potential energy states, the Griffith approach can be recast as a Grand Canonical Monte Carlo (GCMC) approach, in which mass points are randomly removed following a maximum dissipation criterion until the energy release rate reaches the fracture energy.
3. Duality of Local and Global Approaches: The duality of the two approaches was illustrated through the application of the PMF-inspired LEM method for fracture propagation in a homogeneous linear elastic solid using different means of evaluating the energy release rate. It should, however, be noted that a definite proof of the duality between the two approaches remains to be developed. It can be speculated that such a proof could be established by analogy with the ergodicity hypothesis of thermodynamics, according to which the average of a process parameter over time (i.e. fracture surface established by removing bonds, in the local approach, in quasi-static evolutions corresponding to long time scales) and the average over the statistical ensemble (i.e. fracture surface generated, in the global approach, by random mass point removals in a grand canonical ensemble) are the same. A first evidence of this duality has been herein suggested from a comparison of the energy release rates evaluated respectively from the *J*-integral and from the potential energy variation.
4. Computational Efficiency: From an implementation point of view, it can be argued that the local fracture-strength approach is computationally more efficient than the global approach as it requires a smaller amount of energy minimization steps of the system than the GCMC-type global approach which probes a large number of possible energy minima as criterion for mass point removal. While this may hold true for homogeneous and inhomogeneous systems with well-defined microtextures, one could conjecture that the GCMC-approach when properly implemented could turn out more efficient for highly disordered systems exhibiting highly heterogeneous microtextures.
5. Application to Heterogeneous Materials: Considering a textbook example of fracture propagation in an inhomogeneous layered material system, the proposed PMF-inspired LEM approach permits investigating effective fracture properties of heterogeneous materials. Specifically, by benchmarking our LEM results against earlier results (Hossain et al., 2014) obtained by a variational fracture field approach, we confirm that for two-phase layered materials undergo significant toughening mechanisms due to fracture energy contrast, elastic heterogeneity and crack deflection.

With a rational simulation framework thus in place, it is expected that the proposed PMF-inspired fracture LEM approach will be of some help enabling the investigation of 'real'-life highly heterogeneous and multiphase materials as obtained by e.g. X-Ray micro-Computed Tomography such as geological materials (Desrues et al., 2006; Hubler et al., 2017). To this end, the required inputs could be obtained by small-scale characterization techniques such as the scratch test (Akono and Ulm, 2014). This is the focus of forthcoming developments. This method could also be extended for the simulation of dynamic fracturing (Zhao et al., 2011).

Acknowledgments

Research carried out within the X-Shale Hub@MIT, the Science and Engineering of Gas Shale, a collaboration between Shell, Schlumberger and MIT, enabled through MIT's Energy Initiative. FR would like to acknowledge the support of the

ICoME2 Labex (ANR-11-LABX-0053) and the A*MIDEX projects (ANR-11-IDEX-0001-02) cofunded by the French program "Investissements d'Avenir", managed by the French National Research Agency (Agence Nationale de la Recherche). The authors acknowledge Vincent Richefeu (Université Joseph Fourier) and Jean-Yves Delenne (Montpellier SupAgro) who provided the backbone of the LEM code used for the simulations.

Appendix A. Comment on the GCMC method

In fact, in the μVT ensemble, where μ is a prescribed chemical potential, V the constant volume of the structure, and T the absolute temperature, the rules of Grand Canonical probability density for mass point addition read:

$$acc(N \to N+1) = \min\left(1, \frac{V\lambda^{-3}}{N+1}\exp\left(-\beta(\Delta U - \mu)\right)\right), \tag{A.1}$$

and for mass point deletion:

$$acc(N \to N-1) = \min\left(1, \frac{N}{V\lambda^{-3}}\exp\left(-\beta(\Delta U + \mu)\right)\right), \tag{A.2}$$

where $\beta = 1/(k_B T)$ is the Boltzmann factor (k_B is the Boltzmann constant) which amplifies, in function of the absolute temperature T, the difference between the change in energy $\Delta U = U^J - U^I$ between an initial state I and the attempted state J and the chemical potential μ (negative in insertion, positive in deletion). In the classical sense of molecular simulations, $\lambda = h\sqrt{\beta/(2\pi m)}$ stands for the de Broglie wavelength (with h the Planck constant, and $m = \rho a_0^3$ the particle mass), which is required not only for dimensional consistency, but also to anchor the problem within the framework of classical mechanics (in contrast to quantum mechanics), for which $\lambda/a_0 \ll 1$, which is equivalent to restricting the lattice size in the LEM simulations to:

$$a_0 \gg \left(\frac{h^2}{2\pi\rho k_B T}\right)^{1/5}. \tag{A.3}$$

While generally satisfied for the typical temperature range considered in LEM, choosing a $\Lambda = \lambda/a_0 \ll 1$ value for the GCMC simulations, is equivalent to fixing, for a given mass, an equivalent temperature for the simulations, or vice versa fixing the particle mass for a given temperature, that is:

$$T = \frac{h^2}{2\pi k_B m \Lambda^2 a_0^2};\ m = \frac{h^2}{2\pi k_B T \Lambda^2 a_0^2}. \tag{A.4}$$

This temperature–mass scaling has thus an impact on the GCMC simulations via the Boltzmann factor $\beta = 1/(k_B T)$ in the acceptance criteria (A.1) and (A.2).

References

Affes, R., Delenne, J.-Y., Monerie, Y., Radjaï, F., Topin, V., 2012. Tensile strength and fracture of cemented granular aggregates. Eur. Phys. J. E 35, 117.
Akono, A.-T., Ulm, F.-J., 2014. An improved technique for characterizing the fracture toughness via scratch test experiments. Wear 313 (1–2), 117–124.
Ballarini, R., Kayacan, R., Ulm, F.-J., Belytschko, T., Heuer, A., 2005. Biological structures mitigate catastrophic fracture through various strategies. Int. J. Fract. 135, 187–197.
Barenblatt, G., 1962. The mathematical theory of equilibrium cracks in brittle fracture. Adv. Appl. Mech. 7, 55–129.
Bažant, Z., 1984. Size effect in blunt fracture: concrete, rock, metal. J. Eng. Mech. 110, 518–535.
Bolander Jr, J., Saito, S., 1998. Fracture analyses using spring networks with random geometry. Eng. Fract. Mech. 61, 569–591.
Bonamy, D., Bouchaud, E., 2011. Failure of heterogeneous materials : a dynamic phase transition? Phys. Rep. 498, 1–44.
Bourdin, B., Francfort, G., Marigo, J., 2010. The Variational Approach to Fracture. Springer Netherlands.
Bower, A., Ortiz, M., 1991. A three-dimensional analysis of crack trapping and bridging by tough particles. J. Mech. Phys. Solids 39 (6), 815–858.
Brochard, L., Hantal, G., Laubie, H., Ulm, F.-J., Pellenq, R., 2015. Capturing material toughness by molecular simulation: accounting for large yielding effects and limits. Int. J. Fract. 194, 149–167.
Bueckner, H., 1987. Weight functions and fundamental fields for the penny-shaped and the half-plane crack in three-space. Int. J. Solids Struct. 23 (1), 57–93.
Chen, H., Lin, E., Jiao, Y., Liu, Y., 2014. A generalized 2D non-local lattice spring model for fracture simulation. Comput. Mech. 54, 1541–1558.
Chiaia, B., Vervuurt, A., Van Mier, J., 1997. Lattice model evaluation of progressive failure in disordered particle composites. Eng. Fract. Mech. 57, 301–318.
Christoffersen, J., Mehrabadi, M., Nemat-Nasser, S., 1981. Micromechanical description of granular material behavior. J. Appl. Mech. 48, 339–344.
Démery, V., Rosso, a., Ponson, L., 2014. From microstructural features to effective toughness in disordered brittle solids. E 105 (3).
Desrues, J., Viggiani, G., Besuelle, P., 2006. Advances in X-Ray Tomography for Geomaterials. ISTE.
Dugdale, D., 1960. Yielding of steel sheets containing slits. J. Mech. Phys. Solids 8, 100–104.
Faber, K., Evans, A., 1983. Crack deflection processes-I. Theory. Acta Metall. 31, 565–576.
Gao, H., Rice, J., 1989. A first-order perturbation analysis of crack trapping by arrays of obstacles. J. Appl. Mech. 56, 828–836.
Griffith, A., 1921. The phenomena of rupture and flow in solids. Philos. Trans. R. Soc. A 221, 163–198.
Hansen, A., Roux, S., Herrmann, H., 1989. Rupture of central-force lattices. J. Phys. FR 50, 733–744.
He, M.-Y., Hutchinson, J., 1989. Crack deflection at an interface between dissimilar elastic materials. Int. J. Solids Struct. 25, 1053–1067.
Herrmann, H., Roux, S., 1990. Statistical models for the fracture of disordered media. Random Materials and Processes. Elsevier Science.
Hossain, M.Z., Hsueh, C.J., Bourdin, B., Bhattacharya, K., 2014. Effective toughness of heterogeneous media. J. Mech. Phys. Solids 71, 15–32.
Hrennikoff, A., 1941. Solution of problems of elasticity by the framework method. J. Appl. Mech. 12, 169–175.
Hubler, M., Gelb, J., Ulm, F.-J., 2017. Microtexture analysis of gas shale by XRM imaging. J. Nanomech. Micromech. 7 (3).
Hutchinson, J., 1968. Plastic stress and strain fields at a crack tip. J. Mech. Phys. Solids 16, 337–347.
Irwin, G., 1958. Fracture. Springer, Berlin, Heidelberg, pp. 551–590.

Kamat, S., Su, X., Ballarini, R., Heuer, A., 2000. Structural basis for the fracture toughness of the shell of the conch Strombus gigas. Nature 405, 1036–1040.
Kosteski, L., Barrios D'Ambra, R., Iturrioz, I., 2012. Crack propagation in elastic solids using the truss-like discrete element method. Int. J. Fract. 174, 139–161.
Laubie, H., Monfared, S., Radjaï, F., Pellenq, R., Ulm, F.-J., 2017a. Disorder-induced stiffness degradation of highly disordered porous materials. J. Mech. Phys. Solids. (Submitted)
Laubie, H., Monfared, S., Radjaï, F., Pellenq, R., Ulm, F.-J., 2017b. Effective potentials and elastic properties in the lattice element method: isotropy and transverse isotropy. J. Nanomech. Micromech. (Accepted).
Laubie, H., Ulm, F.-J., 2014a. Irwin's conjecture: crack shape adaptability in transversely isotropic solids. J. Mech. Phys. Solids 68, 1–13.
Laubie, H., Ulm, F.-J., 2014b. Plane-strain crack problem in transversely isotropic solids for hydraulic fracturing applications. J. Eng. Mech. 140.
Launey, M., Buehler, M., Ritchie, R., 2010. On the mechanistic origins of toughness in bone. Annu. Rev. Mater. Res. 40, 25–53.
Lilliu, G., van Mier, J., 2003. 3D lattice type fracture model for concrete. Eng. Fract. Mech. 70, 927–941.
Masoero, E., Del Gado, E., Pellenq, R., Yip, S., Ulm, F.-J., 2014. Nano-scale mechanics of colloidal CSH gels. Soft Matter 10, 491–499.
Mohammadipour, A., Willam, K., 2015. Lattice simulations for evaluating interface fracture of masonry composites. Theor. Appl. Fract. Mech. 82, 152–168.
Mohammadipour, A., Willam, K., 2016. Lattice approach in continuum and fracture mechanics. J. Appl. Mech. 83, 1–9.
Monfared, S., Laubie, H., Radjaï, F., Pellenq, R., Ulm, F.-J., 2017. Mesoscale poroelasticity of heterogeneous media. J. Nanomech. Micromech. (Submitted).
Morse, P., 1929. Diatomic molecules according to the wave mechanics. II. Vibrational levels. Phys. Rev. 34, 57–64.
Nayfeh, A., Hefzy, M., 1978. Continuum modeling of three-dimensional truss-like space structures. AIAA 16, 779–787.
Nguyen, T., Yvonnet, J., Zhu, Q.-Z., Bornert, M., Chateau, C., 2015. A phase field method to simulate crack nucleation and propagation in strongly heterogeneous materials from direct imaging of their microstructure. Eng. Fract. Mech. 139, 18–39.
Rice, J., 1968. A path independent integral and the approximate analysis of strain concentration by notches and cracks. J. Appl. Mech. 35, 379–386.
Rice, J., 1985. First-order variation in elastic fields due to variation in location of a planar crack front. J. Appl. Mech. 52, 571–579.
Rice, J., Thomson, R., 1974. Ductile versus brittle behaviour of crystals. Philos. Mag. 29, 73–97.
Schlangen, E., Garboczi, E., 1996. New method for simulating fracture using an elastically uniform random geometry lattice. Int. J. Eng. Sci. 34, 1131–1144.
Schlangen, E., Garboczi, E., 1997. Fracture simulations of concrete using lattice models: computational aspects. Eng. Fract. Mech. 57, 319–332.
Shao, Y., Zhao, H.-P., Feng, X.-Q., Gao, H., 2012. Discontinuous crack-bridging model for fracture toughness analysis of nacre. J. Mech. Phys. Solids 60, 1400–1419.
Shum, D., Hutchinson, J., 1990. On toughening by microcracks. Mech. Mater. 9, 83–91.
Sukumar, N., Dolbow, J., Moës, N., 2015. Extended finite element method in computational fracture mechanics: a retrospective examination. Int. J. Fract. 196, 189–206.
Sun, C.-T., Jin, Z., 2012. Fracture Mechanics. Academic Press, Waltham, MA.
Topin, V., Delenne, J.-Y., Radjaï, F., Brendel, L., Mabille, F., 2007. Strength and failure of cemented granular matter. Eur. Phys. J. E 23, 413–429.
van Mier, J., 1996. Fracture Processes of Concrete. CRC Press.
van Mier, J., van Vliet, M., Wang, T., 2002. Fracture mechanisms in particle composites: statistical aspects in lattice type analysis. Mech. Mater. 34, 705–724.
Zhao, G.-F., Fang, J., Zhao, J., 2011. A 3D distinct lattice spring model for elasticity and dynamic failure. Int. J. Numer. Anal. Methods Geomech. 35, 859–885.